See Retraction Published January 6, 2023

Synthetic lethality of combined glutaminase and Hsp90 inhibition in mTORC1-driven tumor cells

Jing Li[a,1,2], Alfredo Csibi[a,1,3], Sun Yang[b], Gregory R. Hoffman[a,4], Chenggang Li[b], Erik Zhang[b], Jane J. Yu[b], and John Blenis[a,c,5]

[a]Department of Cell Biology, Harvard Medical School, Boston, MA 02115; [b]Division of Pulmonary and Critical Care Medicine, Department of Medicine, Brigham and Women's Hospital, Boston, MA 02115; and [c]Sandra and Edward Meyer Cancer Center, Department of Pharmacology, Weill Cornell Medical College, New York, NY 10021

Edited by Nahum Sonenberg, McGill University, Montreal, QC, Canada, and accepted by the Editorial Board November 25, 2014 (received for review September 3, 2014)

The mammalian target of rapamycin complex 1 (mTORC1) integrates multiple signals from growth factors, nutrients, and cellular energy status to control a wide range of metabolic processes, including mRNA biogenesis; protein, nucleotide, and lipid synthesis; and autophagy. Deregulation of the mTORC1 pathway is found in cancer as well as genetic disorders such as tuberous sclerosis complex (TSC) and sporadic lymphangioleiomyomatosis. Recent studies have shown that the mTORC1 inhibitor rapamycin and its analogs generally suppress proliferation rather than induce apoptosis. Therefore, it is critical to use alternative strategies to induce death of cells with activated mTORC1. In this study, a small-molecule screen has revealed that the combination of glutaminase (GLS) and heat shock protein 90 (Hsp90) inhibitors selectively triggers death of *TSC2*-deficient cells. At a mechanistic level, high mTORC1-driven translation rates in *TSC1/2*-deficient cells, unlike wild-type cells, sensitizes these cells to endoplasmic reticulum (ER) stress. Thus, Hsp90 inhibition drives accumulation of unfolded protein and ER stress. When combining proteotoxic stress with oxidative stress by depletion of the intracellular antioxidant glutathione by GLS inhibition, acute cell death is observed in cells with activated mTORC1 signaling. This study suggests that this combination strategy may have the potential to be developed into a therapeutic use for the treatment of mTORC1-driven tumors.

glutaminase | Hsp90 | mTORC1 | synthetic lethality | inhibitors

The mammalian Target of Rapamycin Complex-1 (mTORC1) is a master regulator of several processes required for cell growth and proliferation, including protein synthesis and autophagy (1). Aberrantly elevated mTORC1 signaling is frequently detected in a large number of genetic tumor syndromes (2), highlighting the potential use of mTORC1 inhibitors in cancer treatment. However, recent clinical trials with mTORC1 inhibitors (rapamycin and its analogs) demonstrated that, although these agents induce tumor shrinkage, tumors grow back upon the cessation of the treatment (3–5). These observations underscore the need to identify additional targets and/or more effective drug combinations. Here, we exploited the unique vulnerabilities of cells with activated mTORC1 by targeting these sensitized processes to selectively induce death. We have focused on a distinct subset of mTORC1-driven tumor cells: those that possess mutations in the Tuberous Sclerosis Complex 2 (TSC2) tumor suppressor gene. The TSC1 and TSC2 gene products form a functional complex that has GTPase-activating protein activity toward Ras homolog enriched in brain to inhibit mTORC1, which is constitutively activated in TSC mutant tumors, such as tuberous sclerosis complex and sporadic lymphangioleiomyomatosis (LAM).

Endoplasmic reticulum (ER) stress is induced when unfolded proteins accumulate in the ER (6). Such stress can be effectively triggered by the inhibition of heat shock protein 90 (Hsp90) chaperones (7). Cancer cells frequently exhibit high levels of ER stress caused by factors such as high mutational load, copy number variation, oxidative stress, and hypoxia (8, 9). To cope with this stress, cells have developed an adaptive signaling pathway known as the unfolded protein response (UPR) or ER stress response. However, if stress is prolonged or severe, the UPR initiates programmed cell death (10). *TSC1*/2-deficient cells are hypersensitive to ER stress due to increased protein synthesis (11, 12). Moreover, activation of the mTORC1 pathway by the loss of *TSC*1/2 renders cells sensitive to energetic stress as a result of metabolic changes (13). Therefore, contrary to current therapies aimed at turning "OFF" the mTORC1 pathway, which would reduce proteotoxic stress, our approach is to induce cell death by taking advantage of the increased protein synthesis and subsequent energy requirements in cells with mTORC1 "ON." To address this possibility and identify new determinants of Hsp90 inhibitor sensitivity, we screened a panel of compounds with either known or proposed roles in cellular metabolism in $Tsc2^{-/-}$ mouse embryonic fibroblasts (MEFs). We found that inhibition of glutaminase (GLS), an enzyme involved in glutamine anaplerosis, potently sensitizes $Tsc2^{-/-}$ cells to Hsp90 inhibition by decreasing the intracellular glutathione (GSH) pool. Importantly, this combination treatment promotes tumor regression of a *Tsc2*-deficient Eker rat uterine leiomyoma-derived (ELT3)-xenograft tumor model. Thus, our study reveals an attractive approach that could

Significance

The mammalian target of rapamycin complex 1 (mTORC1)-mediated signaling regulates protein translation, cell size/growth, cell survival, and metabolism. This signaling is commonly deregulated in cancer as well as genetic disorders such as tuberous sclerosis complex and sporadic lymphangioleiomyomatosis. Recent studies have shown that the mTORC1 inhibitor rapamycin and its analogs generally decrease proliferation rather than inducing cell death. In this study, we found a strategy that rapidly triggers death of cells with activated mTORC1-mediated signaling by using the combination of aminohydrolase enyzme glutaminase and chaperone protein heat shock protein 90 inhibitors. We believe this combination strategy may have potential to be developed into therapeutic use for the treatment of mTORC1-driven tumors.

Author contributions: J.L., A.C., J.J.Y., and J.B. designed research; J.L., A.C., S.Y., C.L., and E.Z. performed research; G.R.H. contributed new reagents/analytic tools; J.L. and A.C. analyzed data; and J.L., A.C., and J.B. wrote the paper.

The authors declare no conflict of interest.

This article is a PNAS Direct Submission. N.S. is a guest editor invited by the Editorial Board.

[1]J.L. and A.C. contributed equally to this work.

[2]Present address: Pfizer, Inc., Cambridge, MA 02139.

[3]Present address: Infinity Pharmaceuticals, Inc., Cambridge, MA 02139.

[4]Present address: Novartis Institutes for Biomedical Research, Cambridge, MA 02139.

[5]To whom correspondence should be addressed. Email: jblenis@med.cornell.edu.

This article contains supporting information online at www.pnas.org/lookup/suppl/doi:10.1073/pnas.1417015112/-/DCSupplemental.

potentially be developed into clinical use for mTORC1-driven cancers with the potential for improved outcomes over cytostatic rapamycin-based therapies.

Results

A Targeted Hsp90 Inhibitor Sensitization Screen in a TSC Cell Line Model. To evaluate the possibility that inhibition of proteins involved in energy metabolism might modulate the cellular response to the Hsp90 inhibitor 17-*N*-allylamino-17-demethoxygeldanamycin (17AAG) and to assess this possibility in a relatively unbiased fashion, we conducted a sensitization screen using 17AAG and a small-molecule library in *Tsc2*$^{-/-}$ MEFs. The library was composed of known inhibitors of glycolysis, glutaminolysis, fatty acids synthesis/oxidation, nucleotide synthesis, and kinase activity (Table S1). 17AAG has been reported to inhibit mTORC1 signaling (14). In agreement, we also observed decreased S6K1 phosphorylation at a high concentration of 1 μM after 72 h of treatment (Fig. 1*A*). To ensure that the mTORC1 was ON, we performed dose–response experiments by assessing the phosphorylation of the ER stress marker [PKR-like ER kinase (PERK) at T980] and the mTORC1 substrate (S6K1 at T389). We found increased phosphorylation of PERK along with sustained S6K1 phosphorylation at a low dose of 0.25 μM 17AAG (Fig. 1*A* and Fig. S1*B*). Accordingly, we performed the screen using 0.3 μM 17AAG, a dose in which we effectively induced ER stress [elevated phosphorylated PERK (P-PERK)] under the condition of sustained mTORC1 activation (high P-S6K1) (Fig. 1*A*). At this concentration of 17AAG, we observed minimum effects on the viability of *Tsc2*$^{-/-}$ MEFs (see Fig. 3*A*). Cells were treated with three different concentrations of small molecules in combination with either 17AAG or the drug vehicle DMSO in a 384-well plate format. After 3 d of continuous culture in the presence of 17AAG, cell viability was determined by using the CellTiter-Glo (Promega), and the effect of compounds on the cellular response to 17AAG was estimated by comparing the viability data between drug- and vehicle-treated plates. After data normalization, we classified the effect of each compound upon 17AAG sensitivity according to fold change in cell viability. As shown by others, taxol (positive control) was found to sensitize *Tsc2*$^{-/-}$ MEF to 17AAG (15). Interestingly, the GLS inhibitor bis-2-(5-phenylacetamido-1,2,4-thiadiazol-2-yl)ethyl sulfide (BPTES) (16) caused the most significant effect (threefold increase) (Fig. 1*B* and Fig. S1*A*). GLS is the enzyme that generates glutamate from glutamine in the first step of a process termed glutamine anaplerosis, which plays

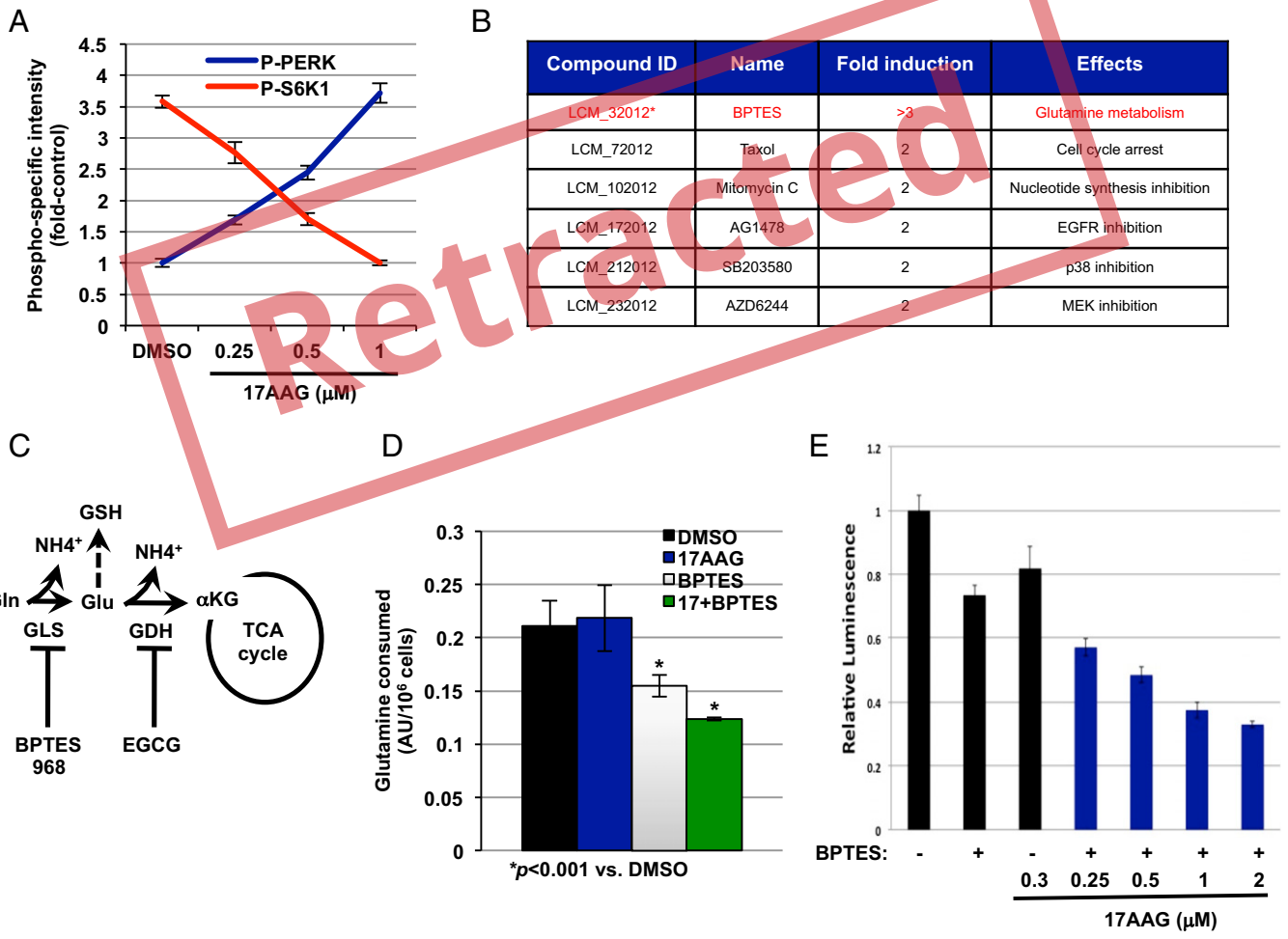

Fig. 1. A targeted small-molecule screen identifies GLS inhibition to sensitize *Tsc2*$^{-/-}$ MEFs to Hsp90 inhibition. (*A*) Phosphospecific intensities for PERK and S6K1 in *Tsc2*$^{-/-}$ MEFs treated with increasing concentrations of 17AAG as indicated for 72 h. The intensities were calculated by using the LiCOR-Odyssey Infrared Imaging system. The mean is shown; error bars represent SEM ($n > 3$). (*B*) Molecules identified to sensitize *Tsc2*$^{-/-}$ to 17AAG (0.3 μM) at a cutoff of twofold. (*C*) A diagram showing the enzymes involved in glutamine anaplerosis and GSH production and the inhibitors used in this study (see text for more details). (*D*) Glutamine consumption of *Tsc2*$^{-/-}$ MEFs after 72 h of treatment with DMSO, 17AAG (0.5 μM), BPTES (10 μM), or BPTES plus 17AAG. The mean is shown; error bars represent SEM ($n > 3$). (*E*) Cell viability of *Tsc2*$^{-/-}$ MEFs using the CellTiter-Glo. Relative luminescence was measured in *Tsc2*$^{-/-}$ MEFs after 72 h of treatment with increasing concentrations of 17AAG with or without BPTES as indicated. The mean is shown; error bars represent SEM ($n > 3$).

a major role in cancer (Fig. 1*C*) (17). Glutamine uptake rates were significantly reduced in BPTES-treated cells (Fig. 1*D*). Importantly, there is an increased sensitivity to BPTES at low concentration of 17AAG starting at 0.25 μM (Fig. 1*E*).

Inhibition of Glutamine Anaplerosis and Hsp90 Causes Potent Apoptosis in *Tsc2*$^{-/-}$ Cells. To assess the magnitude of 17AAG sensitivity in the presence of BPTES on cell viability, we examined cell morphology using microscopy analysis. Phase-contrast imaging confirmed decreased cell viability of *Tsc2*$^{-/-}$ MEFs treated with BPTES plus 17AAG by 48 h. This effect was more pronounced after 72-h treatment compared with single-drug–treated or vehicle-treated cells (Fig. 2*A*). Moreover, to elucidate the biological consequences of combined BPTES and 17AAG, we performed transmission electron microscopy (TEM). Within 24 h, BPTES plus 17AAG induced profound morphological changes of subcellular components (Fig. 2*B*). The dual-combination treatment induced an accumulation of lipid droplets, which are commonly found in cells undergoing apoptosis (Fig. 2*B*) (18). The ER and mitochondria can both act as a source of membranes for autophagosomes (19–21). In our study, BPTES plus 17AAG induced an accumulation of double-membrane autophagosomes (Fig. 2*C*), lysosomes (L), and late endosomes (LE) (Fig. 2*D*), suggesting that the autophagy–lysosomal system is active in cells treated with BPTES and 17AAG. Supporting this idea, we observed a decrease in the level of p62, a marker of autophagy (Fig. S2).

Targeted therapies are anticipated to be more effective in inducing selective death of cancer cells over normal cells. Thus, we compared the viability of *Tsc2*$^{-/-}$ MEFs with *Tsc2*–wild-type (WT) MEFs treated with increasing doses of 17AAG with or without BPTES. Strikingly, the treatment with combined BPTES and 17AAG was more toxic in *Tsc2*$^{-/-}$ MEFs than *Tsc2*–WT at lower doses of 0.25 and 0.5 μM (Fig. 3*A*). Similarly, decreased cell viability with BPTES (10 μM) plus 17AAG (0.25 and 0.5 μM) was also observed in ELT3 cells, but not in TSC2-reexpressing ELT3 cells (Fig. S3*A*). To note, single treatment with 17AAG at a concentration of 1 μM decreased the viability of *Tsc2*$^{-/-}$ MEFs and was not selective when combined with BPTES (Fig. 3*A*). This result is likely due to UPR-induced cell death as a result of excessive ER stress (10), as suggested by the large increase in P-PERK at this concentration (Fig. 1*A*). The increased cell death in *Tsc2*$^{-/-}$ MEFs treated with BPTES plus 17AAG nicely correlated with the cleavage of poly(ADP-ribose) polymerase (PARP), a robust and reliable apoptosis marker (22) (Fig. 3*B* and Fig. S3*C*). In contrast, no obvious cleavage of PARP was detected in *Tsc2*–WT MEFs at these doses (Fig. 3*B*), and the cleavage of PARP was also reduced in *Tsc2*$^{-/-}$-reexpressing *Tsc2* cells (Fig. S3 *D* and *E*). Another GLS inhibitor, molecule 968 (23), also increased sensitivity of *Tsc2*$^{-/-}$ MEFs to 17AAG (Figs. 3*B* and 4*A*). In addition, BPTES treatment yielded similar results in combination with either BIIB021 or AUY922, two structurally unrelated Hsp90 inhibitors (Fig. S3*G*). Finally, the RNA interference (RNAi)-mediated knockdown of GLS in *Tsc2*$^{-/-}$ MEFs induced the cleavage of PARP in the presence of 17AAG (Fig. S3*F*). Together, our data demonstrate a clinically relevant role of GLS during Hsp90 inhibition in *Tsc2*$^{-/-}$ cells.

Hsp90 Inhibition Reverses Rapamycin-Insensitive mTORC1 Phenotypes. Rapamycin has been shown to promote tumor regression when combined with Hsp90 inhibitors in two models of Kras-driven tumors (24). This finding prompted us to assess the efficacy of this combination in our *Tsc2*$^{-/-}$ model in vitro. For this purpose, we treated *Tsc2*$^{-/-}$ MEFs with combined rapamycin (20 ng/mL) and 17AAG (1 μM) for 2 and 24 h. Interestingly, 17AAG was able to abrogate rapamycin-insensitive processes downstream of mTORC1 (Fig. 3C). Accordingly, prolonged rapamycin treatment (24 h) is not able to suppress the mTORC1-dependent phosphorylation of 4EBP1 in a variety of cell lines (25). We reproduced these observations in *Tsc2*$^{-/-}$ MEFs and the patient angiomyolipoma-derived *TSC2*$^{-/-}$ 621-101 cells (Fig. 3*C* and Fig. S3*H*). However, combined

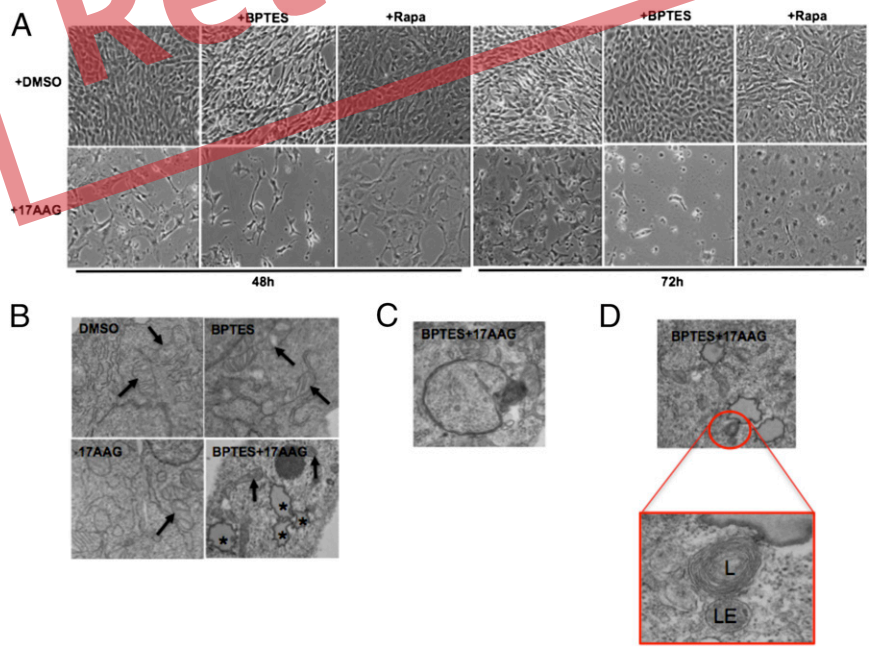

Fig. 2. The combined inhibition of GLS and Hsp90 results in decreased viability and morphological changes of *Tsc2*$^{-/-}$ MEFs. (*A*) *Tsc2*$^{-/-}$ MEFs were treated with DMSO, 17AAG (0.5 μM), rapamycin (20 ng/mL), and BPTES (10 μM) as indicated for 48 and 72 h. Phase microscopy was used to observe cell viability. (*B*) Transmission electron microscopy (TEM) images (9,300 × 1.4×) of *Tsc2*$^{-/-}$ MEFs after 24 h of treatment with DMSO, 17AAG (0.5 μM), BPTES (10 μM), or BPTES plus 17AAG. Black arrows indicate mitochondria, and asterisks indicate lipid droplets. (*C*) TEM image (23,000 × 1.4×) showing a double-membrane autophagosome in *Tsc2*$^{-/-}$ MEFs treated with combined BPTES (10 μM) and 17AAG (0.5 μM). (*D*) TEM images depicting a lysosome (L) and late endosome (LE) in *Tsc2*$^{-/-}$ MEFs treated with combined BPTES (10 μM) and 17AAG (0.5 μM).

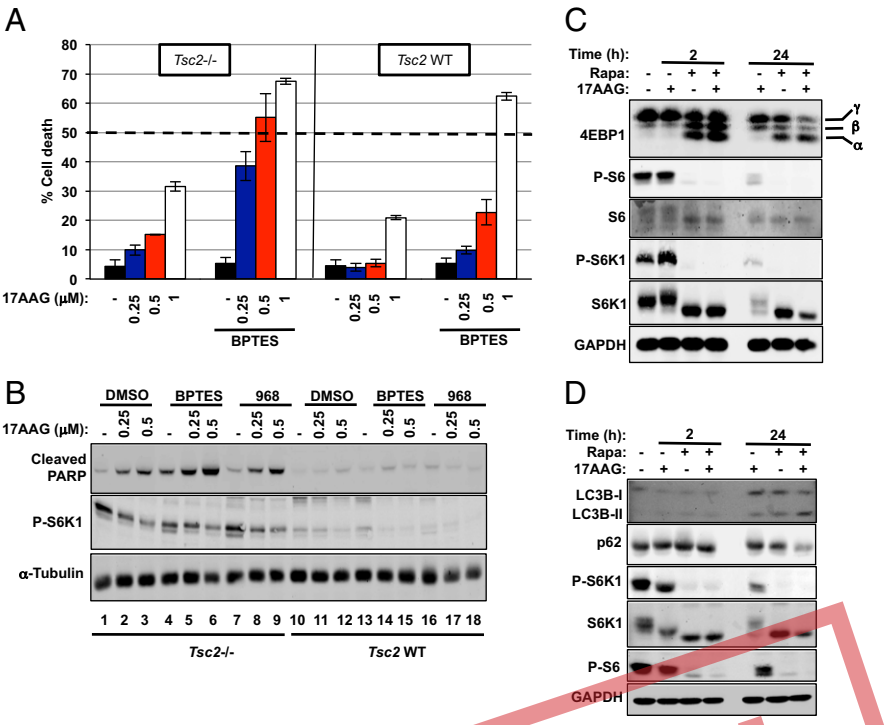

Fig. 3. Inhibition of glutamine anaplerosis and Hsp90 causes potent apoptosis in $Tsc2^{-/-}$ cells. (*A*) Cell death of $Tsc2^{-/-}$ (*Left*) and *Tsc2*–WT (*Right*) MEFs after 72 h of treatment with increasing concentrations of 17AAG with or without BPTES (10 μM) was measured via propidium iodide (PI) exclusion assay. The mean is shown; error bars represent SEM ($n > 3$). (*B*) Immunoblot analysis of cleaved PARP, P-S6K1, 4E-BP1, and α-tubulin in $Tsc2^{-/-}$ MEFs treated with the indicated compounds for 24 h. (*C*) Immunoblot analysis of downstream targets of the mTORC1 pathway in $Tsc2^{-/-}$ MEFs treated with rapamycin (20 ng/mL), 17AAG (1 μM), or the combination of both for the indicated time points. (*D*) Immunoblot analysis of LC3B, p62, P-S6K1, S6K1, P-S6, and GAPDH in $Tsc2^{-/-}$ MEFs treated as in *C*.

17AAG and rapamycin exhibited reduced phosphorylation of 4EBP1 after 24 h of treatment (Fig. 3C and Fig. S3*H*). Moreover, rapamycin is known to mildly induce autophagy in mammalian cells (26). Similar to 4EBP1 de-repression, treatment of $Tsc2^{-/-}$ MEFs with 17AAG plus rapamycin for 24 h resulted in increased cleavage of LC3B (LC3B-II) and decreased p62, two major autophagy markers (Fig. 3*D*). Microscopy analysis revealed that, although proliferation of $Tsc2^{-/-}$ MEFs was decreased after 48 h of treatment with 17AAG plus rapamycin, cells did not grow, but remained viable after 72 h of treatment (Fig. 2*A*). Therefore, this combination seems unlikely to be effective in our model. However, we do not exclude the possibility that a different phenotype might occur in a different cell context or by using specific in vivo systems. Together, these observations support our approach that inducing proteotoxic stress in cells with mTORC1 ON will prove to be more effective at inducing toxicity than when inhibiting the mTORC1 pathway.

Glutamate Dehydrogenase Inhibition Does Not Sensitize Cells to Hsp90 Inhibition. Glutamate, the product of the GLS-catalyzed reaction, is deaminated to generate alpha-ketoglutarate (αKG) by the action of glutamate dehydrogenase (GDH) (Fig. 1*C*). We therefore tested whether epigallocatechin-3-gallate (EGCG), a GDH inhibitor (27), also increased sensitivity to Hsp90 inhibition. We recently validated the action of EGCG on GDH activity in $Tsc2^{-/-}$ MEFs (28). We found that the combination of EGCG and 17AAG neither affected the viability of $Tsc2^{-/-}$ nor induced a significant cleavage of PARP (Fig. 4 *A* and *B*). Similar results were observed in GDH-depleted cells treated (6) with 17AAG (Fig. S4*A*). Thus, our data show a dependency on glutamate to promote cell survival during Hsp90 inhibition. Accordingly, glutamate intracellular levels were significantly reduced in $Tsc2^{-/-}$ MEFs as a result of GLS inhibition or RNAi-mediated GLS silencing (Fig. 4*C*). The addition of glutamate to BPTES plus 17AAG-treated $Tsc2^{-/-}$ MEFs abrogated the induction of apoptosis, as assessed by PARP cleavage (Fig. 4*E*), thus confirming the role of glutamate in the dual-treatment–triggered apoptosis. Nonetheless, we noticed that the addition of glutamate did not completely rescue the viability of the cells (Fig. 4*D* and Fig. S4*B*), which could be due to the permeability and/or stability of glutamate. Alternatively, 17AAG plus BPTES may also affect cysteine and/or glycine metabolism or the key enzymes involved in the synthesis of GSH (see below) (Fig. S5*B*).

As stated above, glutamate serves as a carbon donor for αKG production, an intermediate of the tricarboxylic acid cycle, a metabolic hub with central importance in both energy production and biosynthesis. Importantly, pyruvate and dimethyl-αKG (DM-αKG), a cell-permeable form of αKG, were not able to abolish the cleavage of PARP in BPTES plus 17AAG-treated cells (Fig. 4*F*). Thus, our results suggest that a metabolite derived from glutamate other than αKG is involved in the modulation of cell viability as a result of combined BPTES and 17AAG treatment.

Deregulated Redox Balance Is Responsible for the Apoptosis Induced by BPTES and 17AAG. Besides the role in energy production and macromolecule synthesis, glutamine metabolism (via glutamate) buffers against oxidative damage through GSH, the major intracellular antioxidant (Fig. 5*A*). Glutamine deprivation or RNAi-mediated silencing of GLS suppresses GSH pools and results in increased reactive oxygen species (ROS) (29–31). In agreement with these observations, we found decreased GSH levels in $Tsc2^{-/-}$ MEFs treated with combined BPTES and 17AAG (Fig. 5*B*). The dual treatment also resulted in increased ROS levels compared with single treatments (Fig. 5*C*). ER stress triggers intraluminal calcium release, which promotes mitochondrial membrane depolarization and ROS production (32, 33). ROS further promotes protein misfolding, thereby enhancing ER

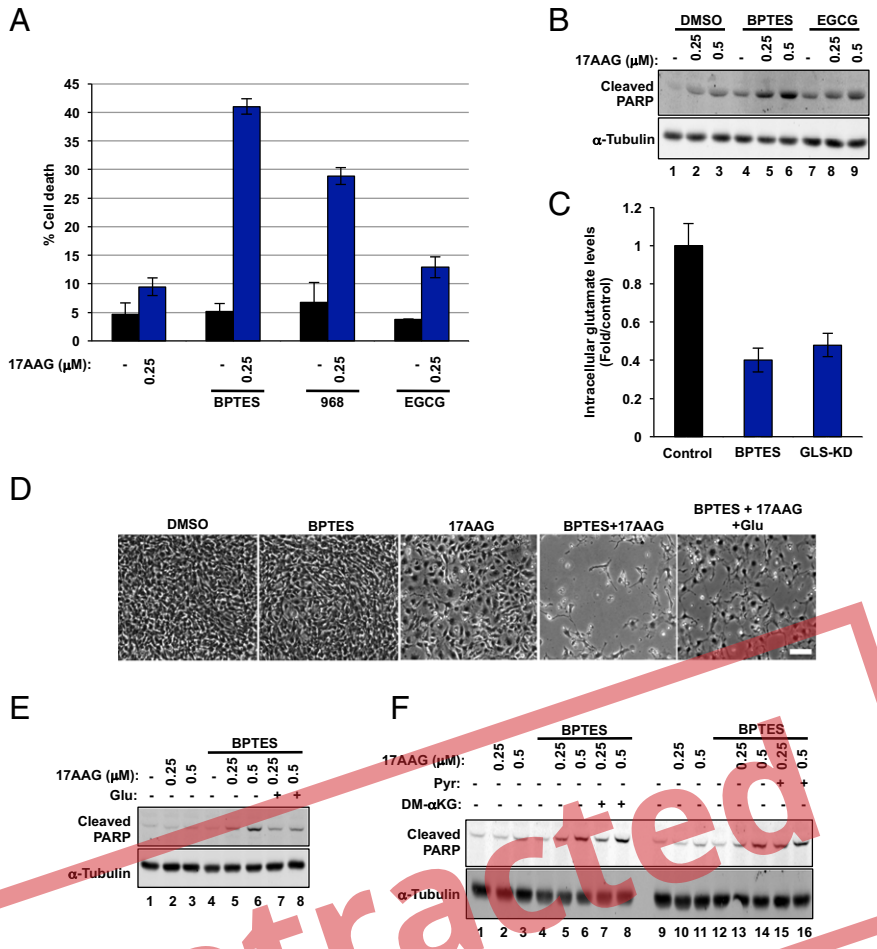

Fig. 4. GDH inhibition does not sensitize cells to Hsp90 inhibition. (*A*) Cell death of *Tsc2*$^{-/-}$ MEFs treated with the indicated compounds for 72 h. The mean is shown; error bars represent SEM ($n > 3$). (*B*) Immunoblot analysis of cleaved PARP and α-tubulin in *Tsc2*$^{-/-}$ MEFs treated as in *A* for 24 h. (*C*) Intracellular glutamate levels in *Tsc2*$^{-/-}$ MEFs treated with BPTES (10 μM) for 72 h. A siRNA targeting GLS was used as a control. The mean is shown; error bars represent SEM ($n = 3$). (*D*) *Tsc2*$^{-/-}$ MEFs were treated with DMSO, 17AAG (0.5 μM), BPTES (10 μM), and glutamate (4 mM) as indicated for 48 h. Phase microscopy was used to observe cell viability. (*E* and *F*) Immunoblot analysis of cleaved PARP and α-tubulin in *Tsc2*$^{-/-}$ MEFs treated with the indicated compounds for 24 h. The concentrations used for the compounds were BPTES (10 μM), glutamate (4 mM), pyruvate (1 mM), and DM-αKG (7 mM).

stress. Consistently, we observed increased phosphorylation of the ER stress marker eIF2α at S151 (Fig. 5*G*, lanes 1–4).

Metabolically active cells are constantly exposed to ROS. Although ROS can initiate signaling events that facilitate both normal and cancer cell proliferation (34), cells must invest heavily to protect themselves against the deleterious effects of pathologically elevated ROS levels (35). These observations suggest that increased ROS levels, as a result of BPTES plus 17AAG, are contributing to the cell death. To assess this hypothesis, we used the antioxidant *N*-acetyl-cysteine (NAC). The addition of NAC rescued the viability of *Tsc2*$^{-/-}$ MEFs treated with BPTES plus 17AAG (Fig. 5*D*). Moreover, another antioxidant, vitamin C, was able to abrogate the cleavage of PARP (Fig. 5*E*) and to rescue the viability of *Tsc2*$^{-/-}$ MEFs (Fig. S4*B*) as a result of the dual combination. Most importantly, GSH monoethylester (GSH-MEE), a cell-permeable form of GSH, abolished the effects of BPTES plus 17AAG on cell death (Fig. 5*F*), thus confirming the essential role of GSH in modulating the viability of stressed *Tsc2*$^{-/-}$ MEFs.

GSH is synthesized through two reactions. First, γ-glutamylcysteine is synthesized from glutamate and cysteine via the glutamate cysteine ligase (GCL). GCL is a heterodimeric enzyme composed of a catalytic (GCLC) and modulatory (GCLM) subunit. GCLC constitutes all of the enzymatic activity, whereas GCLM increases the catalytic efficiency of GCLC. Second, glycine is added to the C-terminal of γ-glutamylcysteine via the enzyme GSH synthetase (GSS) (Fig. 5*A*). The RNAi-mediated knockdown of either GCLC or GSS sensitized *Tsc2*$^{-/-}$ MEFs to Hsp90 inhibition, as evidenced by increased cleavage of PARP. The induction of apoptosis was prevented by treatment with GSH-MEE (Fig. S5*A*). Finally, the GCLC inhibitor buthionine sulfoximine (BSO) induced apoptosis in cells treated with 17AAG (Fig. 5*G*, lanes 6–9).

Dual Inhibition of GLS and Hsp90 Causes Regression of *TSC2*-Deficient ELT3 Cell Xenograft Tumors. To evaluate the role of GLS and Hsp90 inhibition in cells with mTORC1 hyperactivation in vivo, we used an ELT3 cell–xenograft model. We treated mice bearing ELT3–luciferase-expressing xenograft tumors with BPTES and 17AAG as single treatments or in combination. Drug toxicity was first evaluated by body-weight changes, and no obvious effect was observed after the drug treatments (Fig. 6*A*). We next assessed the possible benefits of combination treatment on tumor development and found that xenograft tumor size for 3 wk significantly declined (Fig. 6*B*; $P < 0.05$). Subsequently, in comparison with the vehicle control, single treatment of either BPTES or 17AAG for 3 wk reduced tumor growth by ∼0.35-fold in bioluminescence intensity (Fig. 6 *C* and *D*; $P < 0.05$). More importantly, the combination

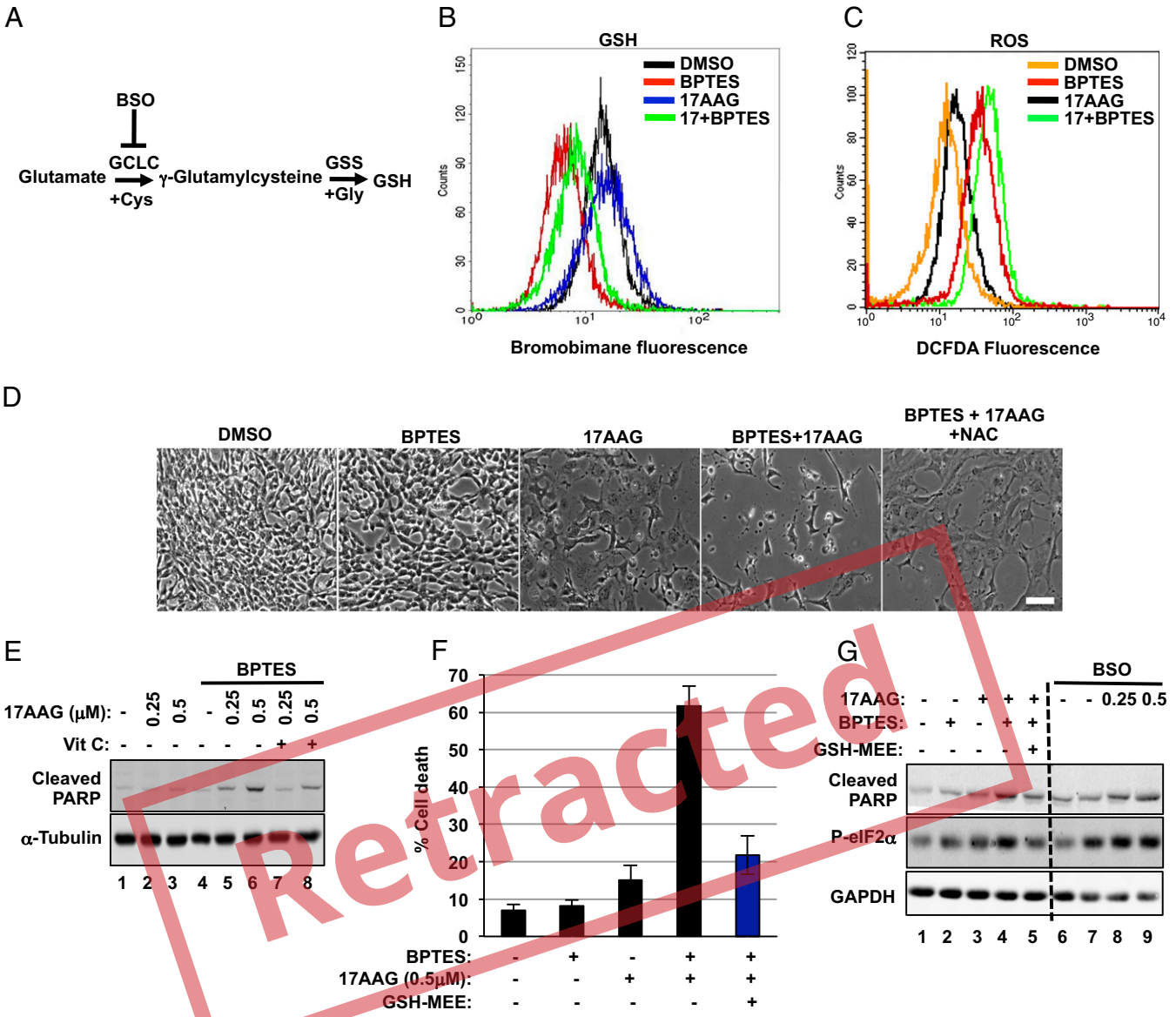

Fig. 5. Deregulated redox balance is responsible for the apoptosis induced by BPTES and 17AAG. (*A*) A diagram showing the enzymes involved in the biosynthesis of GSH and the inhibitor used in this study (see text for more details). (*B*) Intracellular GSH levels were measured in *Tsc2*$^{-/-}$ MEFs treated with DMSO, BPTES (10 μM), 17AAG (0.5 μM), or BPTES plus 17AAG for 48 h ($n = 3$). (*C*) Intracellular ROS levels were measured in *Tsc2*$^{-/-}$ MEFs treated as in *B* ($n = 3$). (*D*) *Tsc2*$^{-/-}$ MEFs were treated with DMSO, 17AAG (0.5 μM), BPTES (10 μM), and NAC (10 mM) as indicated for 72 h. Phase microscopy was used to observe cell viability. (*E*) Immunoblot analysis of cleaved PARP and α-tubulin in *Tsc2*$^{-/-}$ MEFs treated for 24 h with DMSO, 17AAG (0.5 μM), BPTES (10 μM), and vitamin C (100 μM) as indicated. (*F*) Cell death of *Tsc2*$^{-/-}$ MEFs treated with DMSO, 17AAG (0.5 μM), BPTES (10 μM), and GSH-MEE (2 mM) for 72 h. The mean is shown; error bars represent SEM ($n = 3$). (*G*) Immunoblot analysis of cleaved PARP, p-eIF2α, and GAPDH in *Tsc2*$^{-/-}$ MEFs treated for 24 h as in *F* (lanes 1–5) or with BSO (1 mM) combined with increasing concentrations of 17AAG (lanes 6–9).

treatment of BPTES and 17AAG for 3 wk completely suppressed xenograft tumor progression and resulted in tumor regression (Fig. 6 *C* and *D*; $P < 0.05$). Immunohistochemical staining showed that the combination treatment of BPTES and 17AAG resulted in lower levels of cell-proliferation marker proliferating cell nuclear antigen (PCNA), indicating the reduced growth in tumors relative to either agent alone (Fig. 6*E*). We also showed that the combination treatment induces increased apoptotic cell death compared with single-agent treatment using the TUNEL assay (Fig. 6*F*).

Discussion

mTORC1 is an evolutionarily conserved serine/threonine kinase complex that controls cell growth and metabolism in response to nutrients, growth factors, and cellular energy levels. Because numerous oncogenes and tumor suppressors control the activation of mTORC1, deregulation of this pathway is frequently observed in cancers and other diseases. Therefore, targeting the mTORC1 pathway became an attractive therapeutic approach. Preclinical and clinical studies have shown that the mTORC1 inhibitor rapamycin and its analogs are cytostatic rather than cytotoxic. Although rapamycin treatment resulted in decreased tumor size, tumors quickly returned to their initial size shortly after treatment withdrawal (3, 4). Thus, there is an urgent need to develop an alternative way to rapidly induce death in cells with activated mTORC1. In this study, we took an approach by focusing on the observation that cells with activated mTORC1 via the loss of *TSC1/2* are highly sensitive to proteotoxic stress. Our primary goal was to identify new determinants of cell sensitivity

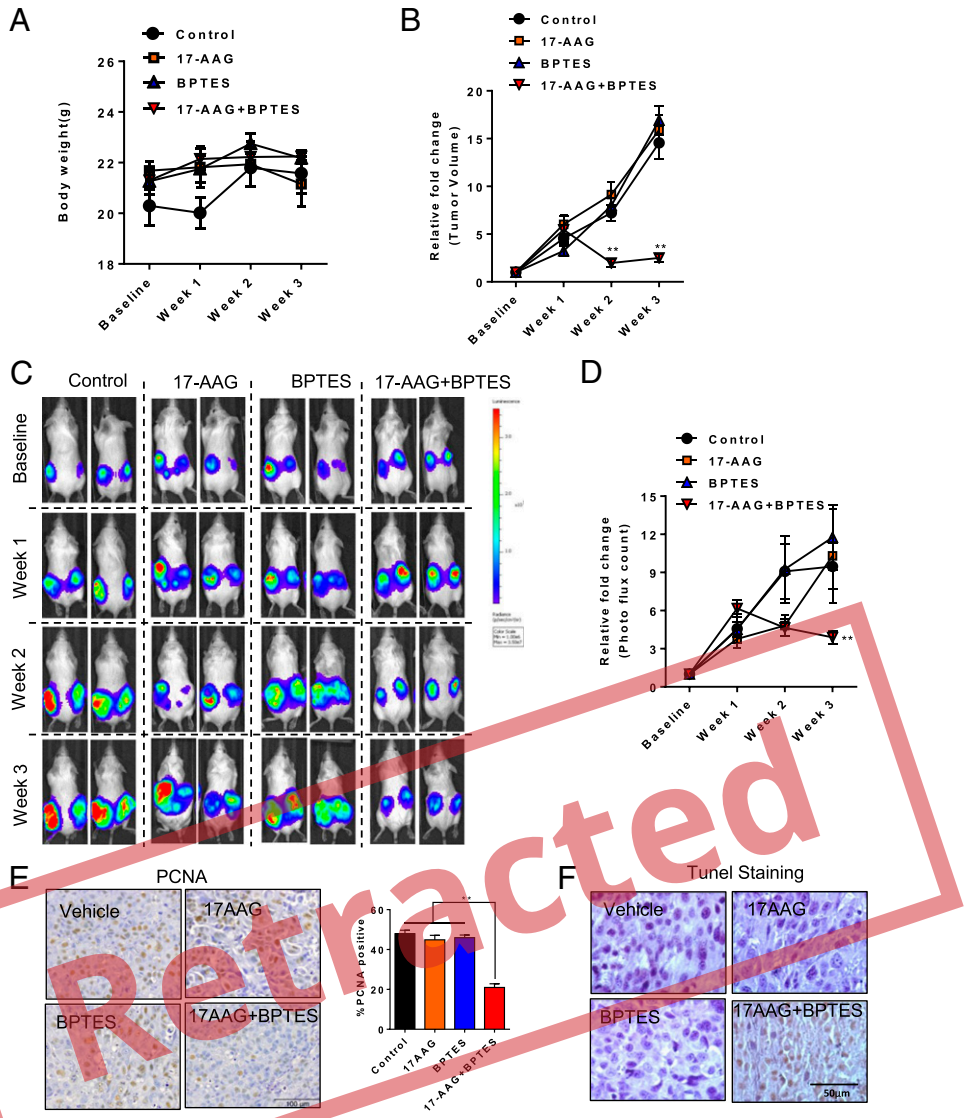

Fig. 6. Dual inhibition of GLS and Hsp90 causes a regression of xenograft tumor development. (*A*) Female CB17-scid mice were inoculated with ELT3-luciferase cells s.c. Mice were treated with vehicle, BPTES, 17AAG, or combined BPTES and 17AAG for 3 wk. Body weight was measured every week. (*B*) Tumor area was measured weekly by using a digital caliper. The left *y* axis indicates the relative fold growth of tumor size vs. the baseline measurement before drug treatment. (*C* and *D*) Bioluminescent intensity in xenograft tumors was recorded and quantified weekly. The left *y* axis indicates the relative tumor growth vs. the baseline quantification before drug treatment. (*E*) Representative images of immunohistochemical staining of cell proliferation marker PCNA in tumors from mice treated with vehicle, BPTES, 17AAG, or combined BPTES and 17AAG. Percentage of cells with nuclear immunoreactivity of PCNA was scored from four to six random fields per section. $^{**}P < 0.01$, Student *t* test. (*F*) Representative images of tumor sections labeled by TUNEL, a method for detecting apoptotic cell death, in tumors from mice treated vehicle, BPTES, 17AAG, or BPTES plus 17AAG.

to Hsp90 inhibitor. Interestingly, through our small-molecule screen, we found that inhibition of GLS sensitizes *Tsc2*$^{-/-}$ cells to Hsp90 inhibition by decreasing the intracellular antioxidant GSH and further increasing the oxidative stress.

Hsp90 inhibition is considered a potential anticancer strategy, and to date, there are 17 distinct Hsp90 inhibitors in clinical trials. Studies have shown that tumors stopped growing when Hsp90 inhibitors were given to animals bearing human tumors. However, similar to rapamycin therapy, the tumors regained their growth capacity after the Hsp90-inhibitor treatment was stopped (36). Therefore, Hsp90 inhibitors or rapamycin may have limited use as a monotherapy. On the contrary, combination therapies offer potential benefits for inhibiting multiple targets and signaling pathways to effectively kill cancer cells and preventing/delaying the emergence of drug resistance (36, 37). The use of combination therapies is supported by recent observations demonstrating that HER2+ breast cancer tumors are more responsive to Hsp90 inhibition when tanespimycin (a geldanamycin analog) was combined with trastuzumab. The effectiveness of this combination could be due to potent target degradation, and it may overcome or delay the initial resistance to trastuzumab (38). De Raedt et al. demonstrated that the combination of rapamycin and Hsp90 inhibitors induced tumor regression in Kras-driven tumor models (24); however, this combination did not seem to be effective in our cell system (Fig. 2*A*). Clinical trials are testing the efficacy of geldanamycin analogs in combination with other chemotherapeutics agents (clinicaltrials.gov/show/NCT01362400).

One other major pitfall with the Hsp90-targeted therapeutics is that Hsp90 also participates in normal cellular physiology, and high doses of these compounds may result in toxicity due to

off-target or increased on-target effects (39). In our combination study, we used low doses of Hsp90 inhibitor that were able to mildly induce the activation of the ER-stress pathway (Fig. 1), while not affecting the viability of the cells. This method could be potentially translated to a better response in the clinic by reducing the toxicity that was previously associated with single treatment. There are several chemically unrelated Hsp90 inhibitors with improved toxicity profiles in the clinical development (39). Thus, it will be interesting to test these structurally distinct inhibitors when combined with GLS inhibitors. Moreover, it will also be worthwhile to identify other specific GLS inhibitors and test their efficacy to sensitize cells to different Hsp90 inhibitors. Glutamine anaplerosis inhibition has recently been shown to result in decreased mTORC1 signaling in the human osteosarcoma cell line U2OS (40). Such an effect was not observed in *Tsc2*$^{-/-}$ MEFs given their constitutive activation of mTORC1 (Fig. 3*B*). However, GLS inhibition resulted in decreased P-S6K1 in *Tsc2*–WT MEFs, which were less sensitive to dual GLS and Hsp90 inhibition (Fig. 3 *A* and *B*), thus supporting the notion that maintaining mTORC1 ON is an effective way to induce cell death. Finally, other agents that enhance ER stress, stimulate ROS production, or inhibit GSH synthesis could also be explored.

We have demonstrated a promising synthetic lethality strategy by targeting Hsp90 and GLS in vitro and in a TSC-xenograft tumor model. Although we used *Tsc2*-deficient cells as a tool to study cells with hyperactive mTORC1, future studies should assess of the efficacy of the combination of GLS and Hsp90 inhibitors in a broader spectrum of cancer cells. We anticipate that this combination approach may have significant benefits in slowing mTORC1-driven tumor progression, including those characterized by the loss- or gain-of-function mutations of upstream regulators of mTORC1, including PTEN and PIK3CA, respectively. Further investigation is warranted to evaluate the therapeutic efficacy.

Experimental Procedures

Cell Lines and Culture. *Tsc2*$^{-/-}$ *p53*$^{-/-}$ and *Tsc2*$^{+/+}$ *p53*$^{-/-}$ MEFs were kindly provided by Brendan Manning and David Kwiatkowski (Harvard Medical School, Boston). ELT3 cells were provided by Cheryl Walker, Texas A&M Health Science Center Institute of Biosciences and Technology, Houston. ELT3-luciferase cells were described (40). MEFs and ELT3 cells were cultured in DMEM supplemented with 10% (vol/vol) FBS (Invitrogen) and dialyzed for experiments (Gibco). All extra energetic additives that are often added to some DMEM formulations such as sodium pyruvate and succinate were excluded. The human renal angiomyolipoma-derived cells (621-101 cells) were cultured in IIA complete medium, 50/50 mixture of Dulbecco's modified Eagle medium/Ham F12 (Sigma D8062) supplemented with sodium selenite (5×10^{-8} mol/L), insulin (25 μg/mL), hydrocortisone (2×10^{-7} mol/L), transferrin (10 μg/mL), triiodothyronine (1×10^{-9} mol/L), vasopressin (10 μU/mL), cholesterol (1×10^{-8} mol/L), ferrous sulfate (1.6×10^{-6} mol/L), epidermal growth factor (10 ng/mL), and 10% FBS.

Small-Molecule Screening. *Tsc2*$^{-/-}$ *p53*$^{-/-}$ MEFs were cultured in DMEM with 10% FBS and penicillin/streptomycin. After overnight culturing, pin-transfer of the small-molecule library was performed at the Institute of Chemistry and Cell Biology-Longwood screening facility. At 72 h after compound addition, the plates were allowed to equilibrate to room temperature for 1 h. Then, 30 μL of CellTiter-Glo (Promega) was added to each well. The plates were allowed to sit for 1 min before being read on the EnVision multilabel plate reader (Perkin-Elmer).

GSH Measurement. Cells grown in 6- or 12-well plates were harvested and trypsinized. The trypsinized cells were then resuspended in 0.5 mL of PBS containing 1% FBS and incubated with 40 μM monobromobimane (Biochemika) for 10 min at room temperature. After incubation, cells were placed on ice, and the fluorescence at 485 nm (blue spectra) was measured by flow cytometry.

Animal Studies. All animal work was performed in accordance with protocols approved by the Children's Hospital Boston Institutional Animal Care and Use Committee.

Statistics. Data were expressed as average ± SEM of at least three independent experiments. An unpaired, two-tailed Student *t* test was used to determine differences between two groups. ANOVA test was used for the analysis of tumor regression among treatment groups.

ACKNOWLEDGMENTS. We thank members of the J.B. laboratory for critical discussions and technical assistance; Alexandra Grassian (Brugge Lab, Harvard Medical School) for help with metabolites measurements; David Kwiatkowski (Brigham and Women's Hospital), Brendan Manning (Harvard School of Public Health), and Takashi Tsukamoto (Johns Hopkins) for providing critical reagents; and the Harvard Medical School Electron Microscopy Facility for advice and assistance with microscopy. J.L. was supported by a Tuberous Sclerosis Alliance Postdoctoral Fellowship. A.C. was supported by a LAM Foundation Postdoctoral Fellowship. C.L. is a LAM Foundation Postdoctoral Fellow. J.B. is a LAM Foundation Established Investigator. This work was supported by National Heart, Lung, and Blood Institute Grant HL098216 (to J.J.Y.) and NIH Grants GM51405 and HL121266 (to J.B.).

1. Ma XM, Blenis J (2009) Molecular mechanisms of mTOR-mediated translational control. *Nat Rev Mol Cell Biol* 10(5):307–318.
2. Menon S, Manning BD (2008) Common corruption of the mTOR signaling network in human tumors. *Oncogene* 27(Suppl 2):S43–S51.
3. Bissler JJ, et al. (2008) Sirolimus for angiomyolipoma in tuberous sclerosis complex or lymphangioleiomyomatosis. *N Engl J Med* 358(2):140–151.
4. Marsh DJ, et al. (2008) Rapamycin treatment for a child with germline PTEN mutation. *Nat Clin Pract Oncol* 5(6):357–361.
5. Li J, Kim SG, Blenis J (2014) Rapamycin: One drug, many effects. *Cell Metab* 19(3):373–379.
6. Ron D, Walter P (2007) Signal integration in the endoplasmic reticulum unfolded protein response. *Nat Rev Mol Cell Biol* 8(7):519–529.
7. Marcu MG, et al. (2002) Heat shock protein 90 modulates the unfolded protein response by stabilizing IRE1alpha. *Mol Cell Biol* 22(24):8506–8513.
8. Luo J, Solimini NL, Elledge SJ (2009) Principles of cancer therapy: Oncogene and non-oncogene addiction. *Cell* 136(5):823–837.
9. Taipale M, Jarosz DF, Lindquist S (2010) HSP90 at the hub of protein homeostasis: Emerging mechanistic insights. *Nat Rev Mol Cell Biol* 11(7):515–528.
10. Tabas I, Ron D (2011) Integrating the mechanisms of apoptosis induced by endoplasmic reticulum stress. *Nat Cell Biol* 13(3):184–190.
11. Ozcan U, et al. (2008) Loss of the tuberous sclerosis complex tumor suppressors triggers the unfolded protein response to regulate insulin signaling and apoptosis. *Mol Cell* 29(5):541–551.
12. Kang YJ, Lu MK, Guan KL (2011) The TSC1 and TSC2 tumor suppressors are required for proper ER stress response and protect cells from ER stress-induced apoptosis. *Cell Death Differ* 18(1):133–144.
13. Choo AY, et al. (2010) Glucose addiction of TSC null cells is caused by failed mTORC1-dependent balancing of metabolic demand with supply. *Mol Cell* 38(4):487–499.
14. Ohji G, et al. (2006) Suppression of the mTOR-raptor signaling pathway by the inhibitor of heat shock protein 90 geldanamycin. *J Biochem* 139(1):129–135.
15. Sain N, et al. (2006) Potentiation of paclitaxel activity by the HSP90 inhibitor 17-allylamino-17-demethoxygeldanamycin in human ovarian carcinoma cell lines with high levels of activated AKT. *Mol Cancer Ther* 5(5):1197–1208.
16. Robinson MM, et al. (2007) Novel mechanism of inhibition of rat kidney-type glutaminase by bis-2-(5-phenylacetamido-1,2,4-thiadiazol-2-yl)ethyl sulfide (BPTES). *Biochem J* 406(3):407–414.
17. Wise DR, Thompson CB (2010) Glutamine addiction: A new therapeutic target in cancer. *Trends Biochem Sci* 35(8):427–433.
18. Boren J, Brindle KM (2012) Apoptosis-induced mitochondrial dysfunction causes cytoplasmic lipid droplet formation. *Cell Death Differ* 19(9):1561–1570.
19. Hayashi-Nishino M, et al. (2009) A subdomain of the endoplasmic reticulum forms a cradle for autophagosome formation. *Nat Cell Biol* 11(12):1433–1437.
20. Ylä-Anttila P, Vihinen H, Jokitalo E, Eskelinen EL (2009) 3D tomography reveals connections between the phagophore and endoplasmic reticulum. *Autophagy* 5(8):1180–1185.
21. Hailey DW, et al. (2010) Mitochondria supply membranes for autophagosome biogenesis during starvation. *Cell* 141(4):656–667.
22. Boulares AH, et al. (1999) Role of poly(ADP-ribose) polymerase (PARP) cleavage in apoptosis. Caspase 3-resistant PARP mutant increases rates of apoptosis in transfected cells. *J Biol Chem* 274(33):22932–22940.
23. Wang JB, et al. (2010) Targeting mitochondrial glutaminase activity inhibits oncogenic transformation. *Cancer Cell* 18(3):207–219.
24. De Raedt T, et al. (2011) Exploiting cancer cell vulnerabilities to develop a combination therapy for ras-driven tumors. *Cancer Cell* 20(3):400–413.
25. Choo AY, Yoon SO, Kim SG, Roux PP, Blenis J (2008) Rapamycin differentially inhibits S6Ks and 4E-BP1 to mediate cell-type-specific repression of mRNA translation. *Proc Natl Acad Sci USA* 105(45):17414–17419.
26. Thoreen CC, Sabatini DM (2009) Rapamycin inhibits mTORC1, but not completely. *Autophagy* 5(5):725–726.

27. Li C, et al. (2006) Green tea polyphenols modulate insulin secretion by inhibiting glutamate dehydrogenase. *J Biol Chem* 281(15):10214–10221.
28. Csibi A, et al. (2013) The mTORC1 pathway stimulates glutamine metabolism and cell proliferation by repressing SIRT4. *Cell* 153(4):840–854.
29. Gao P, et al. (2009) c-Myc suppression of miR-23a/b enhances mitochondrial glutaminase expression and glutamine metabolism. *Nature* 458(7239):762–765.
30. Yuneva M, Zamboni N, Oefner P, Sachidanandam R, Lazebnik Y (2007) Deficiency in glutamine but not glucose induces MYC-dependent apoptosis in human cells. *J Cell Biol* 178(1):93–105.
31. Lora J, et al. (2004) Antisense glutaminase inhibition decreases glutathione antioxidant capacity and increases apoptosis in Ehrlich ascitic tumour cells. *Eur J Biochem* 271(21):4298–4306.
32. Malhotra JD, Kaufman RJ (2007) Endoplasmic reticulum stress and oxidative stress: A vicious cycle or a double-edged sword? *Antioxid Redox Signal* 9(12):2277–2293.
33. Kim J, et al. (2008) Overexpressed cyclophilin B suppresses apoptosis associated with ROS and Ca2+ homeostasis after ER stress. *J Cell Sci* 121(Pt 21):3636–3648.
34. Weinberg F, et al. (2010) Mitochondrial metabolism and ROS generation are essential for Kras-mediated tumorigenicity. *Proc Natl Acad Sci USA* 107(19):8788–8793.
35. Wellen KE, Thompson CB (2010) Cellular metabolic stress: Considering how cells respond to nutrient excess. *Mol Cell* 40(2):323–332.
36. Barrott JJ, Haystead TA (2013) Hsp90, an unlikely ally in the war on cancer. *FEBS J* 280(6):1381–1396.
37. LoRusso PM, et al. (2012) Accelerating cancer therapy development: The importance of combination strategies and collaboration. Summary of an institute of medicine workshop. *Clin Cancer Res* 18(22):6101–6109.
38. Chandarlapaty S, et al. (2010) Inhibitors of HSP90 block p95-HER2 signaling in Trastuzumab-resistant tumors and suppress their growth. *Oncogene* 29(3):325–334.
39. Jhaveri K, Taldone T, Modi S, Chiosis G (2012) Advances in the clinical development of heat shock protein 90 (Hsp90) inhibitors in cancers. *Biochim Biophys Acta* 1823(3):742–755.
40. Durán RV, et al. (2012) Glutaminolysis activates Rag-mTORC1 signaling. *Mol Cell* 47(3):349–358.